

Diffraction-limited Polarimetry from the Infrared Imaging Magnetograph at Big Bear Solar Observatory

WENDA CAO,^{1,2} JU JING,^{1,2} JUN MA,¹ YAN XU,¹ HAIMIN WANG,^{1,2} AND PHILIP R. GOODE^{1,2}

Received 2005 November 28; accepted 2006 April 26; published 2006 June 14

ABSTRACT. The Infrared Imaging Magnetograph (IRIM) system developed by Big Bear Solar Observatory (BBSO) has been put into preliminary operation. It is one of the first imaging spectropolarimeters working at 1565 nm and is used for the observations of the Sun at its opacity minimum, exposing the deepest photospheric layers. The tandem system, which includes a 4.2 nm interference filter, a unique 0.25 nm birefringent Lyot filter, and a Fabry-Pérot etalon, is capable of providing a bandpass as low as 0.01 nm in a telecentric configuration. A fixed quarter-wave plate and a nematic liquid crystal variable retarder are employed for analyzing the circular polarization of the Zeeman components. The longitudinal magnetic field is measured for the highly Zeeman-sensitive Fe I line at 1564.85 nm (Landé factor $g = 3$). The polarimetric data were taken through a field of view of $\sim 145'' \times 145''$ and were recorded by a 1024×1024 pixel, 14 bit HgCdTe CMOS focal plane array camera. Benefiting from the correlation tracking system and a newly developed adaptive optics system, the first imaging polarimetric observations at 1565 nm were made at the diffraction limit on 2005 July 1 using BBSO's 65 cm telescope. After comparing the magnetograms from IRIM with those taken by the Michelson Doppler Imager on board *SOHO*, it was found that all the magnetic features matched very well in both sets of magnetograms. In addition, Stokes V profiles obtained from the Fabry-Pérot etalon scan data provide access to both the true magnetic field strength and the filling factor of the small-scale magnetic flux elements. In this paper, we present the design, fabrication, and calibration of IRIM, as well as the results of the first scientific observations.

1. INTRODUCTION

It has been widely accepted that the small-scale magnetic field concentrations rooted in the deepest layers of solar photosphere play a crucial role in the physical processes driving solar activity and variability. Typical magnetic flux elements are believed to exist in kilogauss-strength magnetic concentrations with a characteristic size of ≤ 100 km at the base of photosphere (Rimmele 2004). The dynamic studies of these flux concentrations require two-dimensional polarimetry with high magnetic sensitivity as well as high spatial and temporal resolution. As a result, two categories of spectropolarimeters have been developed and widely utilized for decades in the observations of the visible wavelengths. The classical spectrograph-based systems are capable of providing high spectral resolution. Since two-dimensional polarimetry is realized by scanning the image across the entrance slit of the spectrograph, these instruments are severely limited in spatial and temporal resolution. Filter-based systems typically offer better spatial resolution, while the moderate spectral resolution is the drawback. However, due to recent advances in Fabry-Pérot interferometer technologies, the spectral resolution $\lambda/\Delta\lambda$ of such

tunable systems can also reach up to $\sim 10^5$ – 10^6 . In the last decade, many Fabry-Pérot-based filter spectropolarimeters operating in the visible wavelength range (Mickey et al. 1996; Bonaccini & Stauffer 1990; Bendlin & Volkmer 1995; Koschinsky et al. 2001; von der Lühe 2000) have demonstrated their importance and bright future. Even so, it is relatively unusual to acquire diffraction-limited observations of small-scale features with subarcsecond spatial resolution and high polarization accuracy (Keller & von der Lühe 1992; Rimmele 2004).

The near-infrared (NIR) provides a promising tool to probe small-scale solar magnetic features, for the following reasons: (1) The Fried parameter, isoplanatic angle, and Greenwood time delay are all proportional to $\lambda^{6/5}$. The angular seeing at 1565 nm is at least 3 times better than in the visible, under the same observational conditions. (2) Zeeman splitting is a function of $g\lambda^2B$. Even a moderate magnetic field can cause full line splitting in the NIR, allowing high-sensitivity measurements of the magnetic field. Meanwhile, the cross talk between the Stokes V and Stokes Q or U components induced by oblique reflections on mirrors in the optical path are considerably suppressed in the NIR. (3) The opacity due to H^- absorption reaches its minimum at 1.6 μm . Therefore, the deepest layers of photosphere can be probed by virtue of this opacity minimum. (4) The scattered light from both the atmosphere and the telescope are extremely reduced in the NIR. The Near-Infrared

¹ Center for Solar-Terrestrial Research, New Jersey Institute of Technology, 323 Martin Luther King Boulevard, Newark, NJ 07102; wcao@bbso.njit.edu.

² Big Bear Solar Observatory, 40386 North Shore Lane, Big Bear City, CA 92314.

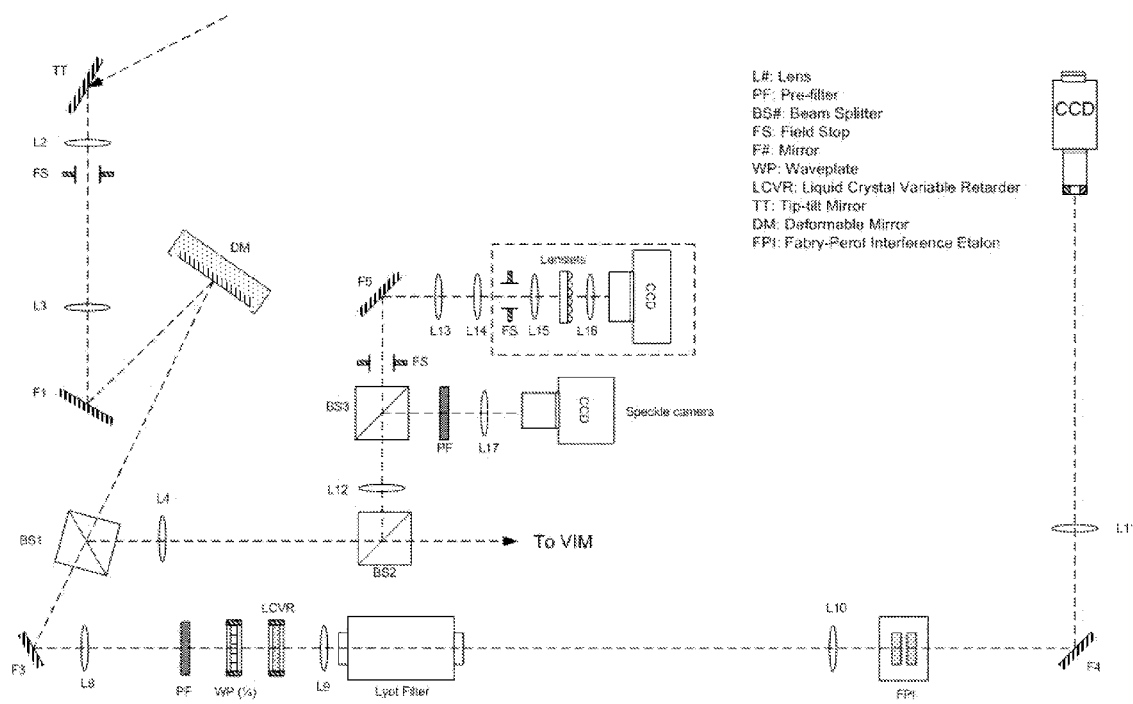


FIG. 1.—Optical layout of BBSO's IRIM and AO systems.

Magnetograph (NIM-I; Rabin 1992a, 1992b) is the first spectrograph-based polarimeter working at 1565 nm, which combines the advantages of infrared Zeeman sensitivity with the capability of spatial mapping. Since then, many NIR spectroscopic and polarimetric observations have been carried out with a variety of spectrographs by a number of authors (Penn et al. 2002, 2003; Bellot Rubio et al. 2000; Lin & Rimmele 1999; McPherson et al. 1992; Solanki et al. 1993; Kopp & Rabin 1992). NIM-II and the dual NIR Fabry-Pérot etalon system of the National Solar Observatory (NSO; Gullixson et al. 1997) are two early attempts at filter-based systems. Despite all of these efforts, only very few reports exist regarding the production of magnetograms by NIR imaging systems, let alone observations made under diffraction-limited conditions.

The Infrared Imaging Magnetograph (IRIM) is one of the first filter-based spectropolarimeters operating in the NIR. Along with the Visible Imaging Magnetograph (VIM) at Big Bear Solar Observatory (BBSO), it will be the most important postfocus instrument of the 65 cm telescope and, in the near future, the 1.6 m New Solar Telescope being developed at BBSO. The design concept has been described by Denker et al. (2003). An interference filter, a birefringent Lyot filter, and a Fabry-Pérot etalon, all working in tandem, are combined to obtain a ~ 0.01 nm bandpass over a field of view (FOV) of $145'' \times 145''$ in a telecentric configuration. The design goal is to acquire images with high spatial resolution (close to the diffraction limit of $\sim 0''.62$), high temporal resolution (~ 1 – 2 minutes), and moderate spectral

resolution ($\sim 10^5$). It will provide four operating modes: polarimeter mode (full spectral profile with polarization optics), spectrometer mode (full spectral profile without polarization optics), Doppler mode (a few selected spectral points), and photometric mode (a single spectral point). After calibrating each optical component, the first diffraction-limited imaging polarimetry using the Fe I 1564.85 nm line was made on 2005 July 1 with the high-order adaptive optics (AO) system of BBSO. In this paper, we present the detailed design of the instrumentation and discuss the preliminary results of the observations.

2. INSTRUMENTATION

The BBSO postfocus instruments, including AO, IRIM, and VIM, are arranged on a stable optical table in a temperature-controlled coude room, with the relevant optical layout shown in Figure 1. A set of relay optics delivers sunlight from the 65 cm telescope into the coude room. The telescope pupil is imaged on a deformable mirror (DM). A dichroic beam splitter (BS1) splits the solar beam reflected by the DM into two individual channels for IRIM and VIM. The beam size is reduced by a positive lens (L8) and a negative lens (L9) from 77 mm to a suitable size to pass through the interference filter, the polarization analyzer, and the birefringent Lyot filter. These two lenses also slow the beam to an f-number of 120 to minimize the bandpass broadening of the Fabry-Pérot etalon. Another positive lens (L10) makes an exact telecentric configuration for the Fabry-

Pérot etalon. An image with a FOV of $145'' \times 145''$ is reimaged onto the focal plane array (FPA) by lens L11.

The NIR detector is a HgCdTe CMOS FPA camera with a TCM8600 image sensor chip manufactured by Rockwell Scientific. The FPA is based on a liquid-nitrogen cooling system and has 1024×1024 pixels, a 100% filling factor, and a quantum efficiency $\geq 50\%$ in the NIR. Eight readout channels ensure a high transfer speed. The characteristic evaluation shows that the maximum transfer rate can reach up to 30 frames s^{-1} (Cao et al. 2005). The output signal is digitized into 14 bits, with a dynamic range better than 70 dB. The pixel size is $18 \mu\text{m} \times 18 \mu\text{m}$.

A 70 mm aperture ET70FS-1041 series II Fabry-Pérot etalon manufactured by Queensgate Instruments, Ltd., is operated by a CS-100 controller (SN 8105) to acquire narrow bandpass transmission and wavelength tunability. To eliminate the impact of fluctuations of ambient pressure, humidity, and temperature, as well as contamination by dust particles, the etalon is mounted in a sealed cell with two antireflection-coated windows. A glass reference capacitor is employed to improve stability in controlling the cavity spacing and etalon parallelism. According to the manufacturer's specifications, the cavity scanning range is larger than 4100 nm, and the reflectivity is over 94% in the wavelength range from 1000 to 1600 nm. Some important performance parameters at 1565 nm have been evaluated and measured by using a He-Ne laser and a horizontal spectrograph, respectively (Cao et al. 2004). The relevant characteristic parameters of IRIM Fabry-Pérot etalon are summarized in Table 1.

As shown in Table 1, the free spectral range (FSR) of the Fabry-Pérot etalon (i.e., the distance between consecutive transmission peaks) is about 0.55 nm at 1565 nm. The birefringent Lyot filter (Wang et al. 2000) was designed to be the order-sorting filter for the Fabry-Pérot etalon. Four stacks of calcite modules sandwiched between linear polarizers are combined to acquire a ~ 0.25 nm bandpass with a diameter of 37 mm. The wide-field configuration used in design tolerates up to a 2° incidence angle. The nematic liquid crystal variable retarders (LCVRs) are attached to each stack and tune the bandpass in a range of ± 10 nm. To avoid a drift of the central bandpass due to variation in the ambient temperature, the whole system is enclosed in a thermal controller. The temperature is maintained at 32°C , with a stability $\pm 0.1^\circ\text{C}$. The calibration and characteristic evaluations were performed by Cao et al. (2006) using the horizontal spectrograph at the NSO Evans Facility at Sacramento Peak. The working voltages of four LCVRs for each stack were determined at 1564.85 nm. The measured FWHM and FSR are 0.246 and 3.975 nm, respectively. The measured transmission is about 15.9% for the unpolarized beam.

A NIR interference prefilter is used to isolate the transmissions from the sidelobe peaks of the birefringent Lyot filter. The transmission profile was measured with the main spectrograph of the NSO McMath-Pierce Telescope at Kitt Peak. The result showed that this three-cavity interference filter provides

TABLE 1
CHARACTERISTIC PARAMETERS OF THE
IRIM FABRY-PÉROT ETALON AT 1565 nm

Parameter	Value
Etalon Properties	
Diameter	70 mm
Rough spacing	2226 μm
Scanning range	4.1 μm
Reflection	95.3%
Absorption	0.27%
Peak transmission	88.8%
Etalon Parameters	
FSR	0.55 nm
Bandpass	8.8 pm
Finesse	62.8
Flatness	$\lambda/127$
Roughness	$\lambda/763$
Step scale	0.29 pm step^{-1}

a bandpass with a FWHM of 4.22 nm, which is able to reduce the sidelobe contamination to a very low level ($<1\%$).

A fixed $\lambda/4$ wave plate, a LCVR, and a NIR linear polarizer constitute the polarization analyzer for measuring the longitudinal magnetic field by using the high Zeeman sensitivity of the Fe I 1564.85 nm line. Because the transmission axis of the five NIR polarizers inside the birefringent Lyot filter are parallel to each other, the filter itself is also a linear polarizer. The fast axis of the fixed $\lambda/4$ wave plate and the LCVR are oriented at 45° to the polarization axis of the birefringent Lyot filter. The left and right circular Zeeman components are converted to orthogonal states of linear polarization by the initial fixed $\lambda/4$ wave plate. The modulator uses a LCVR from Meadowlark Optics, which is electrically switched between 0 and $\lambda/2$. One of the components is blocked by the succeeding linear polarizer, allowing the selected image corresponding to $I + V$ or $I - V$ in the emerging beam. The instrumental polarization of the telescope and other reflecting surfaces has not been modeled; therefore, observations of Stokes Q and U are not possible at this time.

3. OBSERVATIONS

The correlation tracking (CT) system and high-order AO system developed jointly by NSO and BBSO have been put into routine observation (Didkovsky et al. 2003; Rimmele 2000; Rimmele et al. 2003). The CT system uses a 45 mm diameter two-axis tip-tilt mirror with a resonance frequency of around 3.3 kHz and a tilt range of $25''$. The AO system consists of a 77 mm diameter DM with 97 actuators and a Shack-Hartmann wave-front sensor with 76 subapertures. Because of atmospheric stability in the NIR, diffraction-limited polarimetry is often achieved at BBSO over IRIM's FOV in the NIR, while the effect of seeing-induced cross talk is significantly suppressed.

On 2005 July 1, imaging polarimetric observations of NOAA

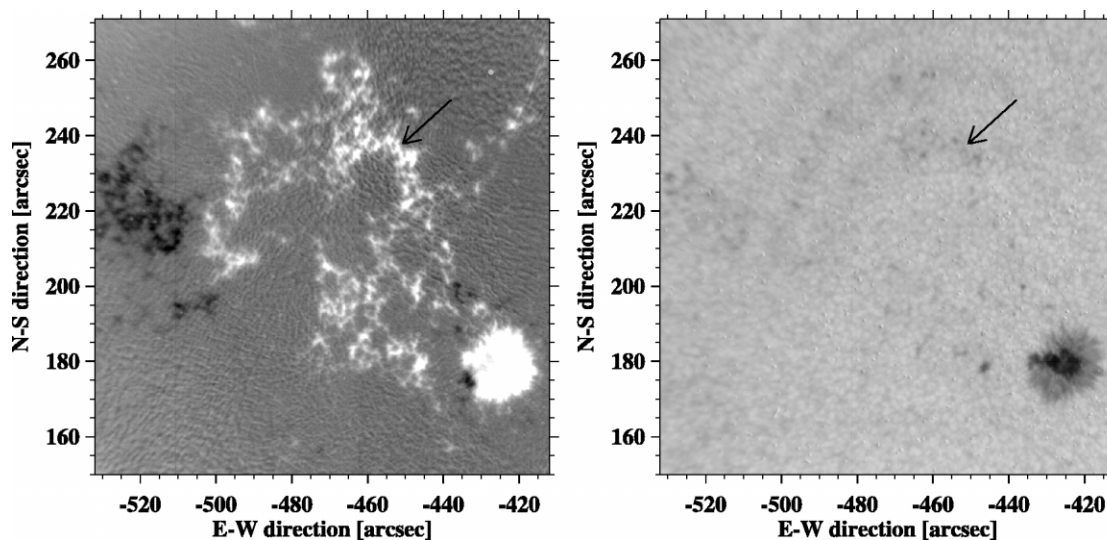


FIG. 2.—*Left*: Magnetogram of NOAA AR 10781 obtained with the BBSO IRIM at 16:02 UT on 2005 July 1. The FOV was $145'' \times 145''$. *Right*: Corresponding image of active region NOAA 10781 taken at the same time. The bandpass is 0.01 nm at 1565 nm.

Active Region 10781 were first made with IRIM, using a combination of the CT and AO systems. The image scale was $0''.142 \text{ pixel}^{-1}$. The data were oversampled by a factor of 2.18 of the diffraction limit at 1565 nm for the BBSO's 65 cm solar telescope. The alternating frames of left- and right-circularly polarized images were acquired by switching the modulator from 0 to $\lambda/2$. These images were stored in separate memory buffers of the image acquisition system. A number of images were added in the respective buffers in order to achieve a sufficiently high signal-to-noise ratio. Because of the high Zeeman sensitivity of the Fe I line at 1564.85 nm, as little as a 40 frame integration is capable of providing a polarization level of $\sim 10^{-4}$. Each image is formed by differencing the above-mentioned component pairs and dividing by their sum. The exposure time is 200 ms for an individual frame. Therefore, each 40 frame integrated Stokes V image at each specific wavelength takes about 20 s. Figure 2 shows a sample magnetogram and the corresponding Stokes I image of NOAA AR 10781 taken at 16:02 UT.

Due to the different Zeeman splitting in distinct solar magnetic features (such as sunspot umbrae, networks, or intra-networks), the corresponding magnetograms reveal different sensitivities at different wavelengths in the same spectral line. It is necessary to search for the most sensitive wavelength region in the blue wing of the spectral line for different targets. Like the old BBSO videomagnetograph, the IRIM bandpass can be fixed at the most sensitive wavelength for tracking rapid changes of these magnetic features. On the other hand, Stokes V profiles can be obtained by scanning magnetograms across the line. These profiles provide the information needed to calculate the true magnetic field strength and the filling factor of the small-scale magnetic features. Hence, IRIM provides two

operating modes for acquiring magnetograms: the single-band-pass mode to monitor rapid magnetic changes, and the scanning mode to obtain the true field strengths.

4. RESULTS

Spectropolarimetric observations of the aforementioned active region were carried out by tuning the Fabry-Pérot etalon from -0.116 nm (blue wing) to $+0.116 \text{ nm}$ (red wing) from the line center, in 5.8 pm steps. The most sensitive response for the network magnetic fields is found when the passband is blueshifted away from the Fe I line center by 0.046 nm. In order to demonstrate the validity of the measurement, we compared our results with the corresponding *SOHO* Michelson Doppler Imager (MDI) magnetograms. Figure 3 shows the MDI magnetogram of NOAA AR 10781 obtained at around the same time. It is very clear that all the magnetic features matched very well in both of the magnetograms. Moreover, the magnetogram from IRIM reveals the small-scale features with sub-arcsecond resolution.

After accurate alignment for each magnetogram at different wavelengths, the Stokes V profile for each resolution element can be constructed. This profile provides an input to measure the true field strength and the filling factor. The inversion of Stokes V profiles for each magnetic element is based on the Unno-Rachkovsky theory. The analytic solution of the transfer equation for polarized radiation for Stokes parameters in a Milne-Eddington atmosphere was first given by Unno (1956) and later by Rachkovsky, who added magneto-optical effects. We used an Unno fitting code in the SolarSoftWare package (`stokesfit.pro`, written by T. R. Metcalf), based on an iterative nonlinear least-squares algorithm to recover the input

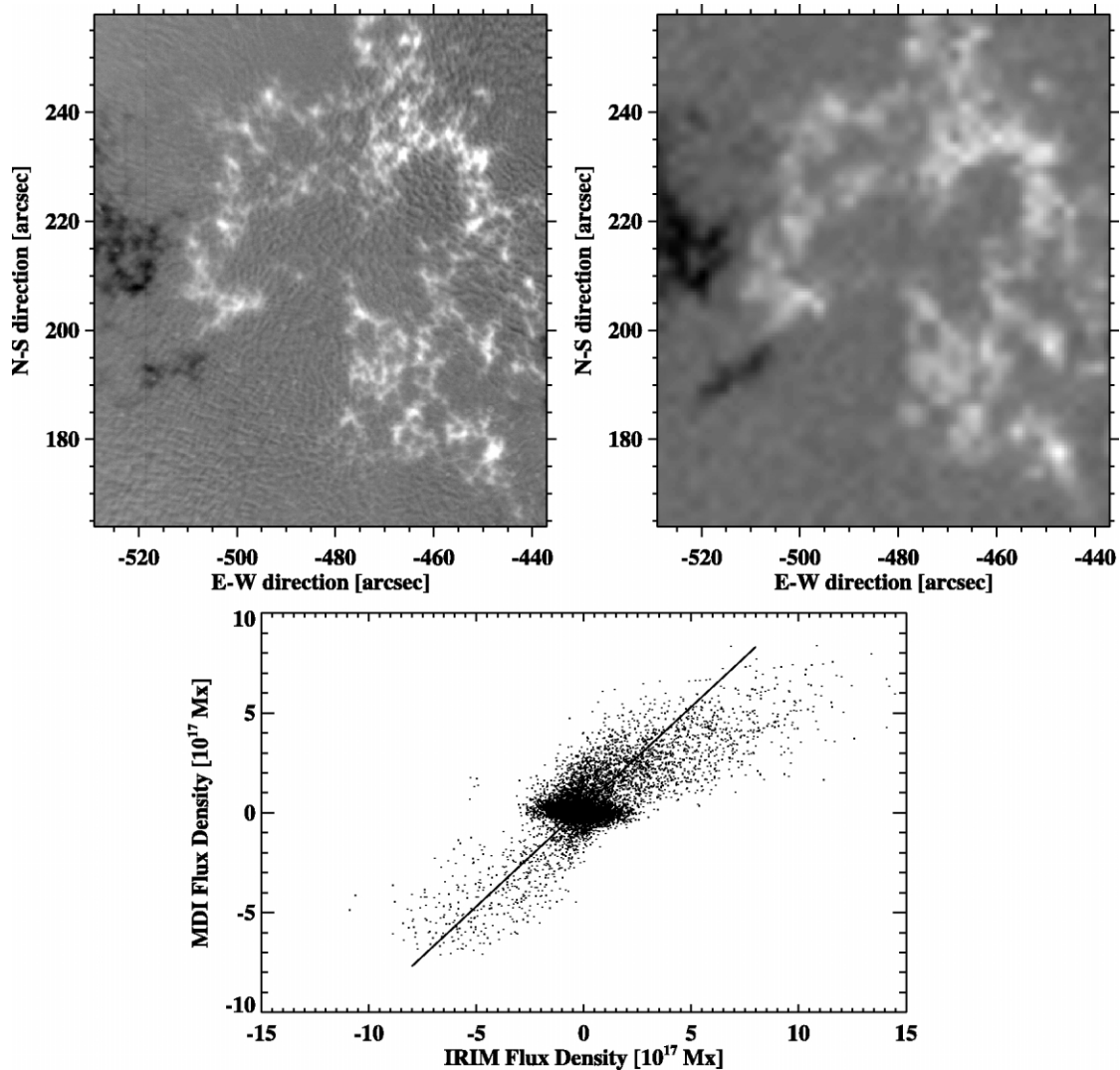


FIG. 3.—*Top*: Magnetograms of NOAA AR 10781 obtained for comparison by IRIM at 16:02 UT (*left*) and MDI at 16:00 UT (*right*). *Bottom*: Scatter plot between IRIM and MDI magnetograms.

magnetic field. The inversion for the magnetic field was performed by minimizing the difference between observed Stokes profiles and those described by the Unno-Rachkovsky solution. Due to the limitation of available LCVRs thus far, only Stokes V and I parameters were measured and included in the fitting. Stokes Q and U variables are ignored in the calculation of χ^2 and the minimization procedure by setting the dummy variables to zero. The fitted results must satisfy the following criteria before being accepted for further analysis: (1) the algorithm must return a covariance matrix of the fitted quantities (i.e., the χ^2 value changes by a convergence tolerance of 10^{-4}); and (2) considering background noise, 2×10^{16} Mx is considered to be the detectable minimum magnetic flux density.

Figure 4 depicts an example of the Stokes V profile over ± 0.116 nm of a magnetic element. The plot corresponds to

the arrows in Figure 2 pointing to the same locations in I and V/I images. The fitted Stokes V profile is also overplotted. The fitted intrinsic magnetic field strength is 482 G, with a filling factor of 49.3%. The inversion procedure was applied to the observed region to obtain the true field, true flux, and filling factor maps of the AR. After making an accurate alignment and degrading IRIM's image scale to match that of MDI, we plotted the scatter diagram, depicted in Figure 3. The plot shows the consistency of two magnetograms from IRIM and MDI. The deviations might be attributed to the use of different spectral lines and differences in spectral and spatial resolution in the two instruments.

This diffraction-limited polarimetry has revealed many dynamic phenomena of small-scale features. Figure 5 shows a detailed example. Although dust on the surfaces of the Fabry-

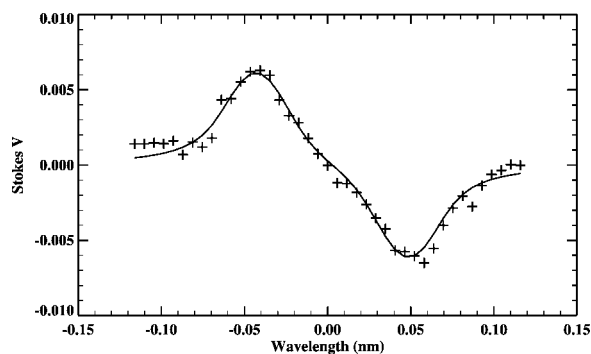


Fig. 4.—Stokes V profile of a small-scale feature indicated by arrows in Fig. 2. The fitted intrinsic field strength is 482 G, with a filling factor of 49.3%, and the corresponding true magnetic flux is 2.04×10^{17} Mx.

Pérot etalon are difficult to clean using dark and flat-field corrections because of the telecentric configuration, some small-scale magnetic features, such as small pores (marked p), magnetic knots (k), etc., are clearly identified in the Stokes I and V/I images in Figure 5. We also found two regions with strong magnetic fields (marked u), yet none corresponding to specific features were discovered in the I image. This discrepancy was also observed by Keller (1995) and Wang et al. (1998). In addition, there is a type of small-scale magnetic structure of special interest (marked e). These features exist in a form of elongated magnetic structure along the dark intergranular lanes, with a characteristic size of $\sim 0''.5 \times 2''$ and a magnetic field of $\sim 150\text{--}300$ G. We will explore the dynamics of these features in more detail in subsequent observations.

5. SUMMARY

An imaging spectropolarimeter based on the Fabry-Pérot etalon has been designed, calibrated, and put into routine observation of Stokes V profiles at the 65 cm telescope at BBSO. This is the first working filter-based magnetograph system in the NIR. The diffraction-limited polarimetry was achieved with the assistance of CT and AO systems using the highly Zeeman-sensitive Fe I line at 1564.85 nm. The comparison of IRIM magnetograms with MDI data illustrates a good consistency between the two. The Stokes V profile from rapid scanning across the spectral line provides the ability to measure the true

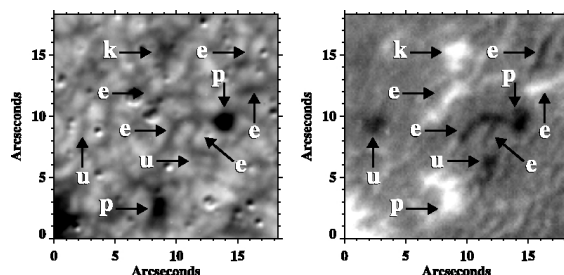


Fig. 5.—Detailed views of small-scale features identified in Fig. 2. *Left*: Stokes I image with a 0.01 nm bandpass at 1565 nm. The dust on the surfaces of the Fabry-Pérot etalon were not cleaned by the dark and flat-field corrections, because of the telecentric configuration. *Right*: Magnetogram taken at the same time. The FOV is $18'' \times 18''$. Small pores (marked by p), magnetic knots (k), magnetic elements without correspondence (u), and elongated magnetic structures (e) are seen clearly, which demonstrates the polarimetry close to the diffraction limit of 65 cm telescope at 1565 nm.

field strength and filling factor using the Stokes inversion method. The preliminary data analysis demonstrates the capability of IRIM to acquire high spatial and temporal resolutions and high Zeeman sensitivity data, which can be used to probe the small-scale dynamic phenomena of the deepest observable levels of the photosphere.

BBSO is building the 1.6 m off-axis New Solar Telescope (NST) to replace the existing telescope, which has a 65 cm aperture. The optical design to upgrade the IRIM to NST is under way. Moreover, a new polarization analyzer system is being fabricated to measure Stokes I , Q , U , and V . In the near future, with the assistance of the NST and AO, the IRIM will offer higher quality polarimetric data with a diffraction-limited resolution ($\sim 0''.25$), high cadence (~ 1 minute), and full Stokes components.

We acknowledge the contributions of C. Denker, J. Wang, K. Hartkorn, T. Spirock, and J. Nenow of BBSO/NJIT. We would also like to thank T. Rimmele at Sacramento Peak/NSO and W. Livingston at Kitt Peak/NSO for their help in the instrument calibration. The authors are grateful to the referee for providing valuable comments. Our work is supported by the NSF under grant ATM 03-42560 and NASA under grant NAS 5-12782.

REFERENCES

- Bellot Rubio, L. R., Collados, M., Ruiz Cobo, B., & Rodríguez Hidalgo, I. 2000, *ApJ*, 534, 989
 Bendlin, C., & Volkmer, R. 1995, *A&AS*, 112, 371
 Bonaccini, D., & Stauffer, F. 1990, *A&A*, 229, 272
 Cao, W., Denker, C., Wang, H., Ma, J., Qu, M., Wang, J., & Goode, P. R. 2004, *Proc. SPIE*, 5171, 307
 Cao, W., Xu, Y., Denker, C., & Wang, H. 2005, *Proc. SPIE*, 5881, 245
 Cao, W., Hartkorn, K., Ma, J., Xu, Y., Spirock, T., Wang, H., & Goode, P. R. 2006, *Sol. Phys.*, in press
 Denker, C., Ma, J., Wang, J., Didkovsky, L., Varsik, J., Wang, H., & Goode, P. R. 2003, *Proc. SPIE*, 4853, 223
 Didkovsky, L. V., et al. 2003, *Proc. SPIE*, 4853, 630
 Gullixson, C., Balasubramaniam, K. S., & Keil, S. 1997, *BAAS*, 29, 897
 Keller, C. U. 1995, *Rev. Mod. Astron.*, 8, 27
 Keller, C. U., & von der Lühe, O. 1992, *A&A*, 261, 321
 Kopp, G. & Rabin, D. 1992, *Sol. Phys.*, 141, 253
 Koschinsky, M., Kneer, F., & Hirzberger, J. 2001, *A&A*, 365, 588

- Lin, H., & Rimmele, T. R. 1999, *ApJ*, 514, 448
- McPherson, M. R., Lin, H., & Kohn, J. R. 1992, *Sol. Phys.*, 139, 255
- Mickey, D. L., Canfield, R. C., LaBonte, B. J., Leka, K. D., Waterson, M. F., & Weber, H. M. 196, *Sol. Phys.*, 168, 229
- Penn, M. J., Cao, W. D., Walton, S. R., Chapman, G. A., & Livingston, W. 2003, *Sol. Phys.*, 215, 87
- Penn, M. J., Ceja, J. A., Bell, E., Frye, G., & Linck, R. 2002, *Sol. Phys.*, 205, 53
- Rabin, D. 1992a, *ApJ*, 390, L103
- . 1992b, *ApJ*, 391, 832
- Rimmele, T. R. 2000, *Proc. SPIE*, 4007, 218
- . 2004, *ApJ*, 604, 906
- Rimmele, T. R., et al. 2003, *Proc. SPIE*, 4839, 635
- Solanki, S. K., Walther, U., & Livingston, W. 1993, *A&A*, 277, 639
- Unno, W. 1956, *PASJ*, 8, 108
- von der Lühe, O., & Kentischer, T. J. 2000, *A&AS*, 146, 499
- Wang, J., Wang, H., Spirock, T. J., Lee, C. Y., Ravindra, N. M., Ma, J., Goode, P. R., & Denker, C. 2000, *Opt. Eng.*, 40, 1016
- Wang, H., et al. 1998, *Sol. Phys.*, 183, 1